

## Identification of novel natural inhibitors of *Opisthorchis felineus* cytochrome P450 using structure-based screening and molecular dynamic simulation

Rohit Shukla<sup>a</sup>, Purna B. Chetri<sup>a</sup>, Amit Sonkar<sup>a</sup>, Maria Y. Pakharukova<sup>b</sup>, Viatcheslav A. Mordvinov<sup>b\*</sup> and Timir Tripathi<sup>a\*</sup>

<sup>a</sup>Molecular and Structural Biophysics Laboratory, Department of Biochemistry, North-Eastern Hill University, Shillong 793022, India; <sup>b</sup>Laboratory of Molecular Mechanisms of Pathological Processes, Institute of Cytology and Genetics, Siberian Branch of the Russian Academy of Sciences, 10 Lavrentiev ave., Novosibirsk 630090, Russia

Communicated by Ramaswamy H. Sarma

(Received 13 September 2017; accepted 6 October 2017)

*Opisthorchis felineus* is the etiological agent of opisthorchiasis in humans. *O. felineus* cytochrome P450 (OfCYP450) is an important enzyme in the parasite xenobiotic metabolism. To identify the potential anti-opisthorchid compound, we conducted a structure-based virtual screening of natural compounds from the ZINC database ( $n = 1,65,869$ ) against the OfCYP450. The ligands were screened against OfCYP450 in four sequential docking modes that resulted in 361 ligands having better docking score. These compounds were evaluated for Lipinski and ADMET prediction, and 10 compounds were found to fit well with re-docking studies. After refinement by docking and drug-likeness analyses, four potential inhibitors (ZINC2358298, ZINC8790946, ZINC70707116, and ZINC85878789) were identified. These ligands with reference compounds (itraconazole and fluconazole) were further subjected to molecular dynamics simulation (MDS) and binding energy analyses to compare the dynamic structure of protein after ligand binding and the stability of the OfCYP450 and bound complexes. The binding energy analyses were also calculated. The results suggested that the compounds had a negative binding energy with  $-259.41$ ,  $-110.09$ ,  $-188.25$ ,  $-163.30$ ,  $-202.10$ , and  $-158.79$  kJ mol<sup>-1</sup> for itraconazole, fluconazole, and compounds with IDs ZINC2358298, ZINC8790946, ZINC70707116, and ZINC85878789, respectively. These lead compounds displayed significant pharmacological and structural properties to be drug candidates. On the basis of MDS results and binding energy analyses, we concluded that ZINC8790946, ZINC70707116, and ZINC85878789 have excellent potential to inhibit OfCYP450.

**Keywords:** *Opisthorchis felineus*; cytochrome P450; virtual screening; drug target; molecular dynamic simulation; natural compounds; molecular docking; binding energy

### 1. Introduction

Opisthorchiasis is a disease caused by the three food-borne trematodes, i.e. *Opisthorchis felineus*, *Opisthorchis viverrini*, and *Clonorchis sinensis*, belonging to the family Opisthorchiidae. These parasites mainly affect the liver and bile duct of humans, animals, and birds (Lim, Mairiang, & Ahn, 2008; Marcos, Terashima, & Gotuzzo, 2008). It has been reported that these parasites have affected over 40 million people in Asia and Europe (Sithithaworn et al., 2007). *O. felineus* is endemic in the territory of the former Soviet Union (Russian Federation (Russia), Ukraine, Belorussia, Kazakhstan, and Baltic countries). *O. viverrini* is widespread in Thailand, Laos, Vietnam, and Cambodia (Sripa et al., 2007), while *C. sinensis* is mainly found in China, Korea, Laos, Vietnam, and in the far-east of Russia (Lun et al., 2005). It has been estimated that up to 600–750 million people are at risk of being infected by these three opisthorchids. *O. felineus* infection is mainly due to the consumption of

raw or undercooked fish infested with larvae. In humans, the symptoms of opisthorchiasis range from asymptomatic to severe. In some regions, such as Ukraine, Russia, and Siberia, where people frequently consume raw fish, the bile ducts have been found to contain high numbers of worms that induce chronic infection characterized by dyspepsia, dryness, and bitter taste in the mouth, fatigue, intolerance for greasy foods, nausea, anorexia, and pain in the right hypochondrium (Mordvinov & Furman, 2010). The chronic infection becomes severe in individuals with a high worm infestation and is characterized by obstruction of bile duct with jaundice, recurrent cholangitis, acute pancreatitis, bile peritonitis, and hepatic abscesses (Mordvinov & Furman, 2010). Presently, praziquantel (PZQ) is the drug of choice for the treatment of opisthorchiasis, clonorchiasis, schistosomiasis, and other trematodiasis (Maule & Marks, 2006; Pakharukova, Shilov, Pirozhkova, Katokhin, & Mordvinov, 2015). However, there are several reports of low sensitivity to

\*Corresponding authors. Email: [mordvin@bionet.nsc.ru](mailto:mordvin@bionet.nsc.ru) (V.A. Mordvinov); [timir.tripathi@gmail.com](mailto:timir.tripathi@gmail.com), [tripathi@nehu.ac.in](mailto:tripathi@nehu.ac.in) (T. Tripathi)

PZQ among these parasites, and the appearance of resistance isolates against this drug emphasizes the need for new drugs (Maule & Marks, 2006). The exact mode of action of PZQ is not known at present, but evidence indicates that PZQ increases the permeability of the membranes of schistosome cells toward  $\text{Ca}^{++}$  ions. The drug thereby induces contraction of the parasites, resulting in paralysis in the contracted state (Mas-Coma, Bargues, & Valero, 2005; Tchuente, Shaw, Polla, Cioli, & Vercruyse, 2004; WHO, 2008).

To understand the basic metabolic systems in flatworms, it is important to understand the adaptation of biochemical systems in parasites, e.g. the mechanisms of their resistance to anthelmintic therapy. An example of such biochemical adaptations in parasites is the simplification of the basic metabolic system – the monooxygenase system of cytochrome P450 (CYP450) (Devine et al., 2010). CYP450 forms an enzyme superfamily that is ubiquitously distributed in nature and represents one of the largest and oldest gene superfamilies (Degtyarenko & Archakov, 1993; Klingenberg, 1958). They are heme-thiolate binding proteins, where the protoporphyrin IX of heme is linked to the apo-protein by a bond between the heme iron center and sulfur atom of a conserved Cys residue of the protein. This enzyme acts as an active component of monooxygenase system in the living organism and displays a variety of biological function ranging from degradation and synthesis of endogenous signaling molecules to detoxification of environmental carcinogens (Nebert & Russell, 2002). In mammals, CYP450s are involved in multiple roles such as the metabolism of drugs and xenobiotic compounds, synthesis of steroid hormones, metabolism of fat soluble vitamins, and conversion of polyunsaturated fatty acids to biologically active molecules (Denisov, Makris, Sligar, & Schlichting, 2005). More than 80% of drugs undergo the steps of biotransformation mediated by CYP450. CYP450s are also functionally important for the survival of invading pathogens. In addition, this enzyme is linked to the synthesis of unique sterol like metabolites, such as oxysterols and catechol estrogen, known specifically from *O. viverrini* and *Schistosoma haematobium* (Gouveia et al., 2013; Vale et al., 2013). It is also essential for worm survival and egg development, and blocking its function would lead to worm death and/or hampering of parasite development (Ziniel et al., 2015). The parasitic flatworms including liver flukes (Opisthorchiidae, Fasciolidae), blood flukes (Schistosomatidae), and cestodes (Taeniidae) contain a single CYP450 gene (Pakharukova et al., 2012, 2015). In these parasites, genes for flavin monooxygenase are absent, and CYP450 acts as the main enzyme with monooxygenase activity toward xenobiotics (Pakharukova, Vavilin et al., 2015). It was found that certain azole inhibitors like ketoconazole, miconazole, and clotrimazole inhibited

the activity of CYP450 enzyme. CYP450 may be the promising drug target against trematodiasis for the development of therapeutic agents (Mordvinov, Shilov, & Pakharukova, 2017; Pakharukova & Mordvinov, 2016).

Current drug discovery process involves the identification of compounds having significant inhibition of target parasitic proteins that are different from its human counterpart and optimization of the identified hits to increase their selectivity, affinity, efficacy, metabolic stability, and bioavailability. Because of the availability of huge numbers of compounds, the high-throughput screening (HTS) process is extremely time-consuming and tedious. Structure-based virtual screening is a much faster computational equivalent of HTS. In the present study, we used the natural compounds from the ZINC database and performed in-depth computational studies that included modeling, structure-based virtual screening, docking, molecular simulations, and binding energy analyses to identify the potential inhibitors of *O. felineus* CYP450 (OfCYP450). The sequential representation of the methodology is shown in Figure 1.

## 2. Methods

### 2.1. Homology modeling and structure validation

OfCYP450 sequence (accession number: F8UVH3) was submitted to PDB-BLAST to determine the closely related homologs. From Protein Data Bank (PDB) we did not find any appropriate sequence for prediction of a homology model. So, OfCYP450 sequence was submitted to I-TASSER server for prediction of a 3D protein model. I-TASSER is an *Ab-initio* server that uses fold recognition methods and predicts a reliable structure. The server predicted best five structures with binding sites information. One best structure on the basis of TM-score was selected and employed for structure validation. After that the structure was employed for 50-ns MDS study to predict a least energy structure. Predicted model and least structure from MDS was validated by structure alignment using ProSA (Wiederstein & Sippl, 2007), ERRAT, PDBsum (Laskowski et al., 1997), and verify3D (Bowie, Luthy, & Eisenberg, 1991; Luthy, Bowie, & Eisenberg, 1992) servers.

### 2.2. Cavity prediction and binding site analysis

The Molegro Virtual Docker (MVD) 2007.2.0.0 (Thomsen & Christensen, 2006) was used for the prediction of the binding sites. For cavity prediction, we used Molegro Molecular Visualizer (MMV). MMV was also used to visualize the hydrogen bonding, electrostatic, and steric interactions of ligands with OfCYP450. Key catalytic residues like Ser118, Asn119, Glu305, Ala309, Thr313, Val351, Leu355, Ala308, Leu446, and Thr447

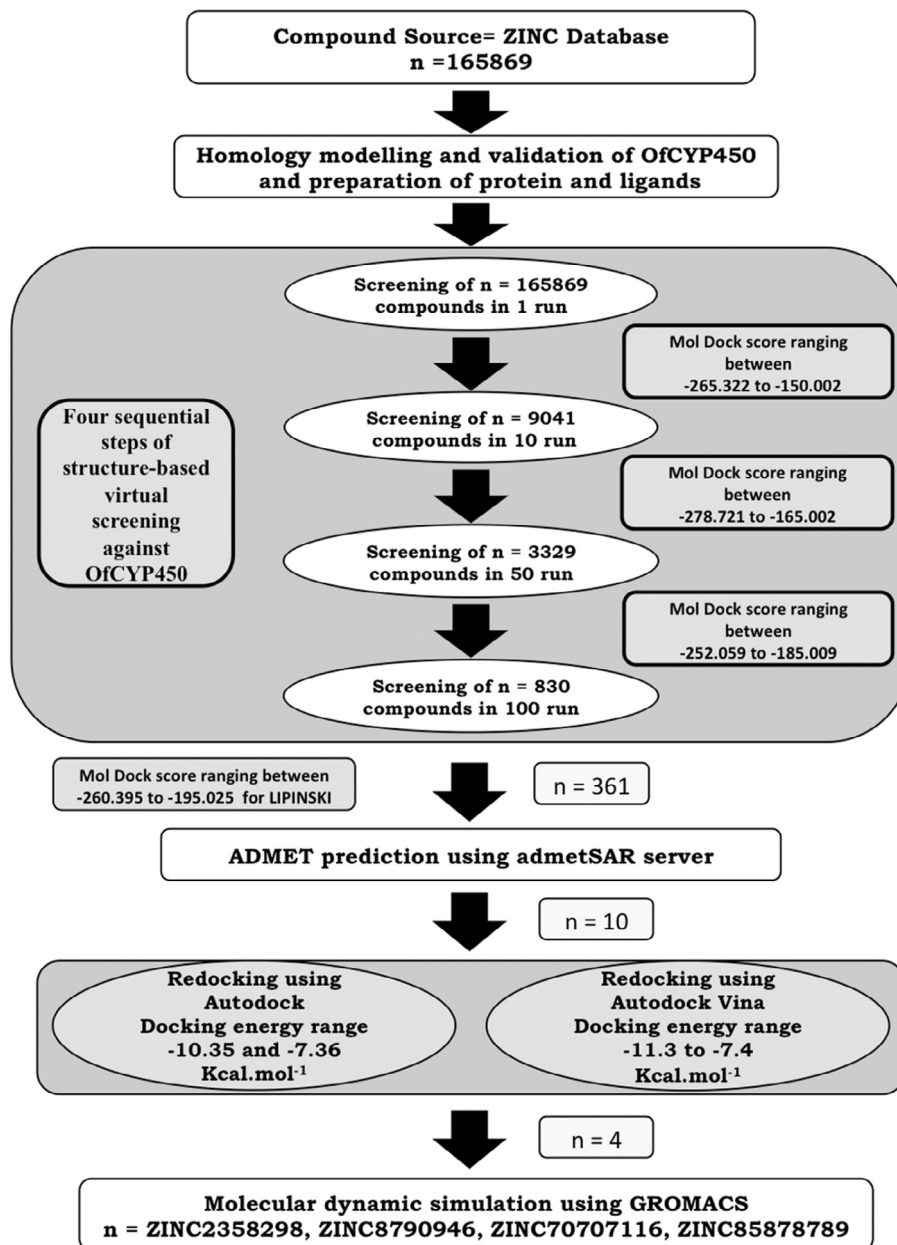


Figure 1. Summary of the overall workflow.

from OfCYP450 were taken as the predicted amino acids for virtual screening (DeVore et al., 2012; Reynald, Sansen, Stout, & Johnson, 2012; Schoch et al., 2008; Wilderman, Shah, Jang, Stout, & Halpert, 2013).

### 2.3. Virtual screening

To identify more efficient inhibitors, virtual screening was carried out in a hierarchical manner involving several steps, starting with a preliminary docking process to identify binding compounds and their subsequent

refining and re-ranking on the basis of docking using several algorithms. The sequence of these steps is summarized in Figure 1. Prior to the virtual screening, the protein structure was prepared using MVD (Thomsen & Christensen, 2006). Molegro is an effective tool for protein–ligand docking as it performs flexible docking by which the ideal geometry of ligand is determined during the docking. The complexes having the energetically favorable structure were selected. MVD calculated the interaction energies between ligands and protein. The MolDock Score was used for energy calculation.

In the study, 1,65,869 natural compounds (a comprehensive subset) were retrieved from ZINC database and screened against the structure of OfCYP450. The cavity used for virtual screening had the size constraint of 13 Å. The docking parameters for virtual screening included the number of runs (1), population size (50), max iterations (2000), scaling factor (0.50), and crossover rate (0.90). From the first round of screening, 9041 compounds were selected for the next screening step. In the second step, all the parameters were kept the same except the number of runs, which was increased from 1 to 10. Increasing the number of runs during screening step removes the false positive binders. From the second round of screening, we selected 3329 compounds for next step screening and runs were increased from 10 to 20. From this round, finally 830 compounds were selected and screened in 50 runs.

#### 2.4. ADMET prediction

The ADMET properties are very important for approving a drug. The prediction of ADMET properties of the compounds as possible drug candidates was performed using admetSAR (Cheng et al., 2012). It predicts physically significant descriptors and pharmaceutically relevant properties of compounds. admetSAR has 95,629 compounds in its data-set that are approved by FDA and are used to predict the main features for ADMET. In this study, several features including blood–brain barrier (BBB), human intestinal absorption (HIA), P-gp substrate/inhibitor, Caco-2 permeability, plasma protein binding, cytochrome p450 (CYP450) substrate/inhibitor, human Ether-a-go-go-Related Gene (hERG) inhibition, AMES toxicity, carcinogenicity, and biodegradability were predicted by the admetSAR server. Total 361 compounds used for ADMET prediction, we found 10 compounds that were suitable as lead compounds and ADMET filters.

#### 2.5. Docking analysis

All the selected 10 compounds and the reference compounds were further docked by Autodock (Goodsell, Morris, & Olson, 1996) and Autodock Vina (Trott & Olson, 2010). Autodock is extensively used software for protein–ligand docking. Same binding pocket was selected for docking studies that was used in virtual screening. Autodock uses the semi-empirical free energy force field for the calculation of ligand-binding conformations. The OfCYP450 structure and ligands were prepared using AutoDock1.5.6. Hydrogen atoms were added to the structure of OfCYP450, and partial atomic charges were assigned. A 3D grid box for docking was set into  $X = 40^\circ$ ,  $Y = 42^\circ$ ,  $Z = 40^\circ$  grid points, and the grid spacing was 0.636 Å. The binding poses were

generated by Lamarckian Genetic Algorithm. Other docking parameters were population size (150), maximum number of evaluations (25,00,000), maximum number of generations (27,000), rate of gene mutation (0.02), and rate of crossover (0.8). All other parameters were kept as default. Fifty binding poses were generated for each ligand. The results were clustered according to the RMSD values and ranked by the binding free energy. Ultimately, Autodock Vina was used for redocking studies. The defined grid for Autodock was considered for docking of the 10 compounds with reference inhibitors by Autodock Vina.

#### 2.6. Molecular dynamics simulation (MDS)

GROMACS 4.6.5 (B. Hess, Kutzner, van der Spoel, & Lindahl, 2008; Pronk et al., 2013) was used to perform MDS in an *in house* supercomputer as earlier (Pandey et al., 2016; Pathak et al., 2017; Shukla, Shukla, Sonkar, & Pandey, 2017; Shukla, Shukla, Sonkar, Pandey, & Tripathi, 2017; Shukla, Shukla, Sonkar, & Tripathi, 2017; Sonkar et al., 2017). Seven systems with reference compounds (itraconazole and fluconazole) were created and used for 50-ns MDS studies, one for predicting the stable structure of the apo-OfCYP and others for OfCYP–ligand bound complexes. All the systems were solvated using simple point charge model in a cubic box. Ligand topology was generated using ProDRG server (Schuttelkopf & van Aalten, 2004). Protein topology was generated using GROMOS 9653a6 force field (Oostenbrink, Villa, Mark, & Van Gunsteren, 2004). Six  $\text{Cl}^-$  ions were added for neutralization of the systems. Steepest energy minimization was performed for all the systems to give the maximum force below  $1000 \text{ kJ mol}^{-1}$  for removing the steric clashes. Long range electrostatic interactions were calculated by particle mesh Ewald (PME) method (Darden, York, & Pedersen, 1993). For the computation of Lennard–Jones and Coulomb interactions, 1.0-nm radius cut-off was used. The LINCS algorithm (Berk Hess, Bekker, Berendsen, & Fraaije, 1997) was used to constrain the hydrogen bond lengths. The time step was maintained at 2 fs for the simulation. For predicting the short-range non-bonded interaction, 10-Å cut-off distance was used. A 1.6-Å Fourier grid spacing was used for the PME method for long-range electrostatics. All bonds including hydrogen bonds were fixed by Shake algorithm (Ryckaert, Ciccotti, & Berendsen, 1977). The systems were equilibrated after energy minimization. Then, position restraint simulation of 1 ns was carried out under NVT and NPT conditions. Finally, all systems were submitted for 50-ns MDS. A 2-fs interval was given for saving the coordinates. Then the root mean square deviation (RMSD), root mean square fluctuation (RMSF), radius of gyration (Rg), and hydrogen bonds were calculated by  $g\_rms$ ,  $g\_rmsf$ ,



g\_gyrate, and g\_hbond tools. The trajectories were analyzed by visual molecular dynamics (Humphrey, Dalke, & Schulten, 1996) and Chimera 1.10.2 (Pettersen et al., 2004). Ultimately, Origin 6.0 was used for generating and visualizing the plots.

### 2.7. Principal component analysis (PCA)

To investigate the conformational dynamics and collective motions upon ligand binding, PCA was performed. The PCA method was embedded in the GROMACS software package (Amadei et al., 1993). After eliminating the rotational and translational movements, coordinates were superimposed onto a reference structure from which the positional covariance matrix of atomic coordinates and its eigenvectors were calculated. Then, diagonalization was performed on the calculated symmetric matrix by an orthogonal coordinate transformation matrix that generated the diagonal matrix of eigenvalues. In this diagonal matrix, columns were the eigenvectors corresponding to the direction of motion relative to the initial coordinates. Each eigenvector was associated with an eigenvalue that represented the total mean square fluctuation of the system along the corresponding eigenvector. The g\_anaeig and g\_covar tools were used for PCA.

### 2.8. Binding free energy calculation

The binding energy of protein–ligand complexes was calculated using the molecular mechanics Poisson–Boltzmann surface area (MM-PBSA) method (Baker, Sept, Joseph, Holst, & McCammon, 2001; Kumari, Kumar, & Lynn, 2014). The free energy analysis is valuable in the advanced stage of drug discovery process. Free energy of solvation (polar + non-polar solvation energies) and molecular mechanics potential energy (electro-static + Van der Waals interaction) were calculated by this tool. In this study, the last 10 ns of the MD trajectories were taken for the calculation of MM-PBSA.

## 3. Results and discussion

### 3.1. Homology modeling and structure validation

The OfCYP450 structure is not available in PDB. Lack of the structure in PDB offers to predict a good 3D structure using different approaches. Homology modeling is the best way to obtain a 3D structure. So, we submitted the sequence of OfCYP450 in PDB for searching a closely related homolog. We did not find relevant sequence similarity of OfCYP450 with any PDB structure using BLASTp. The BLAST result showed < 25% identity with PDB structures. So, we used *ab-initio* approach for protein modeling. I-TASSER is widely used software for structure prediction on the basis of fold, so

I-TASSER server was used for the prediction of the 3D structure of OfCYP450. Five models were predicted by I-TASSER. The model was selected on the basis of C-score, which was calculated based on the significance of threading template alignments and the convergence parameters of the structure assembly simulations. The stereochemical parameters were predicted by ProSA, ERRAT, Verify-3D, and Ramachandran plots. The ProSA, ERRAT, and Verify-3D showed  $-7.58$ ,  $65.055$ , and  $78.40$  scores, respectively (Supplementary Figure S1–S3). The energy plot showed some of the residues with higher positive values (Supplementary Figure S3). The Ramachandran plot showed that 72.9 and 24.4% residues lie in the most favored region and additionally allowed region, respectively. Comparatively, 1.5 and 1.2% residues lie in generously allowed region and disallowed region, respectively (Supplementary Figure S4). All the parameters suggested that predicted model was not good for virtual screening. So for predicting a stable structure, the model was employed for 50-ns molecular dynamics simulation (MDS) study. The MDS result was clustered for predicting a stable structure using Chimera 1.10.2. Following the MDS study, one structure was taken and all the stereochemical parameters were again predicted. The ProSA, ERRAT, and Verify-3D showed  $-7.94$ ,  $88.000$ , and  $77.32$  scores, respectively. The energy plot also showed most of the residues with negative values (Supplementary Figure S3). The Ramachandran plot showed that 86.1 and 11.5% residues lie in the most favored region and additionally allowed region, respectively, while only 1.7 and 0.7% residues lie in generously allowed region and disallowed region, respectively (Supplementary Figure S4). The stereochemical parameters are given in Table 1. All these parameters suggested that the predicted model is refined and can be used for virtual screening study.

### 3.2. Virtual screening

Screening of compounds against a receptor is a very effective way of predicting the best compounds. We retrieved the primary and secondary metabolites subsets from ZINC database. A multi-step virtual screening approach for 1,65,869 compounds against OfCYP450 was used. The protein and ligands were prepared using Molegro Virtual Docker (MVD). All the ligands were screened in one run in the first round. The highest and lowest MolDock scores in the first round were recorded as  $-265.322$  to positive score. We also found that ZINC95100338 showed the highest MolDock score of  $-265.322$ . From the first round screening, 9041 compounds were selected that had MolDock scores between  $-265.322$  and  $-150.002$ . All these compounds were employed for the second round of screening in 10 runs. In this round, ZINC95100379 was found to be the top

Table 1. Stereochemical parameters of the target enzyme.

Structure name	ProSA Z-score	Energy plot	Verify 3D (%)	ERRAT	Ramachandran plot (%)
Modeled OfCyp450	-7.58	Higher	78.40	65.055	72.9, 24.4, 1.5, 1.2
Refined OfCyp450	-7.94	Lower	77.32	88.000	86.1, 11.5, 1.7, 0.7

compound in the terms of the highest MolDock score of -278.721. From this round, 3329 compounds were selected that had MolDock scores between -278.721 and -165.002. After this step, the selected compounds were employed for a third round of screening in 20 runs. In this round, we found that ZINC53276076 showed the highest MolDock score of -252.059. Then, for the next round of screening, we selected 830 compounds that had MolDock scores between -252.059 and -185.009. In this round, ZINC3983911 showed the highest MolDock score of -260.395. Then, these compounds were finally screened for 50 runs. From the last round of screening, 361 compounds that had MolDock scores between -260.395 and -195.025 were selected for ADMET prediction.

### 3.3. In silico pharmacokinetics, metabolism, and toxicity studies

The success of a drug's passage through the body is measured through absorption, distribution, metabolism, elimination, and toxicity (ADMET). The results for these pharmacokinetics parameters were obtained for top hits from virtual screening by calculating the different descriptors. All the selected 361 compounds from virtual screening were employed for prediction of ADMET descriptors.

Blood-brain barrier (BBB) is an important factor for drugs that have the target site in the central nervous system. BBB is a physiological barrier, which protects the compounds to cross from blood to brain. In our study, we observed that out of 361 compounds, 235 compounds had the capability to cross the BBB, while 126 compounds failed. Human intestinal absorption (HIA) describes the absorption of a compound in the gastrointestinal tract. Out of the 361 compounds, 319 compounds showed novel absorption in the intestine, while 42 compounds failed to absorb in the HIA. Caco-2 cell line permeability defines the capability of a compound to permeable from large intestine. Eighty-nine out of 361 compounds passed Caco-2 permeability filter, while 272 compounds failed in this criteria. P-glycoprotein (P-gp) is one of the most important cell surface proteins involved in the efflux of xenobiotics. The substrate of P-gp indicates that the compound can be effluxed by these cell surface proteins. Non-substrate indicated that this

compound could not be effluxed by P-gp cell surface protein. Out of the 361 compounds, 266 compounds acted as a P-gp substrate, while 95 were non-substrates. P-gp inhibitor and non-inhibitor compounds have the capability to inhibit and non-inhibit the P-gp cell surface protein, respectively. Out of the 361 compounds, 180 compounds acted as a non-inhibitor, while 181 acted as an inhibitor of P-gp (Supplementary Table S1). Cytochrome P450 is the major enzyme that play key role in drug metabolism. The admetSAR server predicted Cyp450-substrate and Cyp450-inhibitor. In our study, 183 compounds showed a high inhibition, while 178 compounds showed a low inhibition for CYP450 enzymes (Supplementary Table S2). Toxicity describes how a compound is poisonous or harmful for an organism. In our study, 45 compounds were found to be toxic, while 316 compounds were non-toxic in nature. Carcinogenicity of a compound describes that the compound can cause cancer. In our study, we found that 24 compounds can act as a carcinogen, while 337 compounds were non-carcinogenic. The biodegradability of a compound is a very important parameter. In our study, 21 compounds showed to be readily biodegradable, while 340 showed non-biodegradable property. The hERG codes a channel protein that has the capability to conduct electrical current across the cell membrane and is inhibited by several compounds resulting in long QT syndrome. In our study, we found that 61 compounds acted as an inhibitor, while 300 as non-inhibitor of hERG. The LD<sub>50</sub> of a compound describes the ability of a compound to kill 50% population of an organism. Less and high LD<sub>50</sub> denoted high and low efficacy of the compound, respectively. In our case, most compounds showed the LD<sub>50</sub> value ranging between 2 and 3 mol.Kg<sup>-1</sup> in rat model (Supplementary Table S3). From the overall ADMET studies, we selected 10 compounds for docking that showed excellent values in ADMET descriptors.

### 3.4. Molecular docking study

From the ADMET results, we predicted 10 compounds that were suitable for lead prediction. All these 10 compounds with reference compounds were further docked by Autodock, Autodock Vina, and MVD. The reference compound itraconazole showed a binding affinity of -9.12, -9.8 Kcal.mol<sup>-1</sup> from Autodock to Autodock

Vina, respectively, while MVD showed  $-162.92$  MolDock Score. The other reference compound fluconazole showed a binding affinity of  $-5.4$ ,  $-7.8$  Kcal.mol $^{-1}$  from Autodock to Autodock Vina, respectively, while MVD showed  $-115.01$  MolDock Score.

From Autodock, we predicted that ZINC2358298 showed the highest binding affinity of  $-10.35$  Kcal.mol $^{-1}$ , while ZINC70707655 showed the lowest binding affinity of  $-7.36$  Kcal.mol $^{-1}$ . From Autodock Vina, we observed that ZINC2358298 showed  $-11.3$  Kcal.mol $^{-1}$ , while ZINC70707655 showed  $-7.4$  Kcal.mol $^{-1}$  binding affinity. From Autodock and Autodock Vina, the ZINC70707655 was found with the highest and lowest binding affinities. While in MVD, a different result was observed because MVD used a different algorithm to produce the MolDock score. In MVD, ZINC70707116 showed the highest MolDock score of  $-200.96$ , and ZINC85878789 showed the lowest MolDock score of  $-179.82$ .

From all the three software, we observed that the interacting residues were similar while the docking energy differed less among each other. The interacting residues, number of hydrogen bonds and binding affinity has been provided in the Supplementary Table S4. The structure, binding affinity, and ZINC ID of top four selected compounds with reference ligands are shown in Table 2.

### 3.5. Analysis of the docked complexes

#### 3.5.1. Itraconazole

Itraconazole interacted with several residues and formed two hydrogen bonds with Asn222 and Gly410, with an energy complex of  $-9.12$  Kcal.mol $^{-1}$  by Autodock. Additionally, itraconazole complex stabilized by hydrophobic interactions with Arg98, Val100, Arg102, Leu105, Ser106, Val107, Phe248, Asn250, Asp312, Thr313, His345, Val351, His357, Phe400, Leu402, Gly403, Ala404, Arg405, Ser406, Cys407, Gly409, Leu446, and Thr447. The complex predicted by Autodock Vina was stabilized by one hydrogen bond with Ala404. Additionally, Arg102, Leu105, Ser106, Val107, Asn222, Leu230, Asn250, Asp312, Thr313, Val351, His357, Leu402, Gly403, Arg405, Ser406, Cys407, Gly410, Leu446, and Thr447 were found to participate in the hydrophobic interactions. The binding energy of the complex was  $-9.8$  Kcal.mol $^{-1}$  when calculated by Autodock Vina. In MVD analysis, itraconazole formed one hydrogen bond with Ala404 with an energy complex of  $-162.92$  MolDock score. Here, the residues Arg102, Leu105, Ser106, Val107, Asn108, Asn119, Asp312, Thr313, Thr317, Ile344, His345, Val350, Val351, Phe400, Ser401, Gly403, Cys407, Gly410, and Asp414 were involved in hydrophobic interactions.

The residues Arg102, Leu105, Ser106, Val107, Asp312, Thr313, Val351, Gly403, and Cys407 were found to be common residues interacting with itraconazole studied by all three docking tools. The interactions of OfCYP450–itraconazole complex from Autodock are shown in Supplementary Figure S5.

#### 3.5.2. Fluconazole

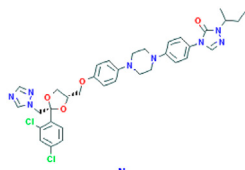
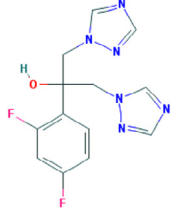
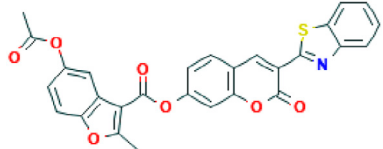
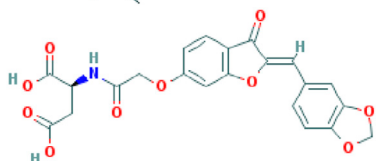
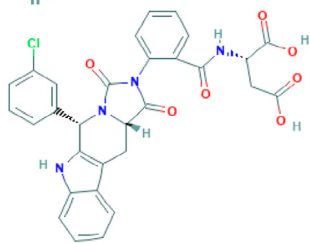
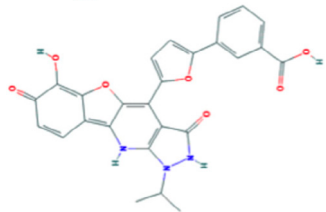
Fluconazole formed three hydrogen bonds with Val350, Ser401, and Ala404 with an energy complex of  $-5.4$  Kcal.mol $^{-1}$  by Autodock. Additionally, fluconazole complex was found to be stabilized by hydrophobic interactions with Thr317, Ile344, His345, Ser349, Val351, and Asn414. The complex predicted by Autodock Vina was stabilized by two hydrogen bonds with Arg102, Asn218. Additionally, Leu105, Ser106, Val107, Asn108, Ser118, Asn222, Ala308, Asp312, Val351, Ala404, Leu446, and Thr447 were found to participate in the hydrophobic interactions. The binding energy of the complex was  $-7.8$  Kcal.mol $^{-1}$  when calculated by Autodock Vina. In MVD analysis, fluconazole formed two hydrogen bonds with Ile344, Val351 with the formation of an energy complex of  $-115.01$  MolDock score. Here, the residues, Thr313, Thr317, His345, Ser349, Val350, Ser401, Gly410, and Asn414, were involved in hydrophobic interactions.

A single residue Val351 was found to be common residue interacting with fluconazole studied by all three docking tools. The interactions of OfCYP450–fluconazole complex from Autodock are shown in Supplementary Figure S5.

#### 3.5.3. ZINC2358298

ZINC2358298 showed the highest binding affinity as compared to other ligands against OfCYP450. ZINC2358298 interacted with several residues and formed five hydrogen bonds with Arg102, Ala104, Cys407, and Val350, with an energy complex of  $-10.35$  Kcal.mol $^{-1}$  by Autodock. Additionally, ZINC2358298 complex was found to be stabilized by hydrophobic interactions with Leu105, Ser106, Val107, Asn108, Ser118, Thr313, His345, Ser349, Val351, and Ser401. The complex predicted by Autodock Vina was stabilized by three hydrogen bonds with Val350, Val351, and Cys407. Additionally, Arg102, Ser106, Val107, Asn108, Asp312, Thr313, His345, Ser349, Ser401, Ala404, and Gly410 were found to participate in the hydrophobic interactions. The binding energy of the complex was  $-11.3$  Kcal.mol $^{-1}$  when calculated by Autodock Vina. In MVD analysis, ZINC2358298 formed five hydrogen bonds with Arg102, Val350, Val351, Ser401, and Cys407 with the formation of an energy complex of  $-189.23$  MolDock score. Here, the residues Leu105,

Table 2. Details of the selected hits.

Compound	Structure	Autodock (Kcal.mol <sup>-1</sup> )	Autodock Vina (Kcal.mol <sup>-1</sup> )	MVD MolDock score
Ttraconazole		-9.12	-9.8	-162.92
Fluconazole		-5.4	-7.8	-115.01
ZINC2358298		-10.35	-11.3	-189.23
ZINC8790946		-9.03	-9.4	-194.18
ZINC70707116		-10.02	-8.3	-200.96
ZINC85879789		-9.57	-10.9	-179.82

Source: ZINC database code, structure, and docking energies obtained after virtual screening and refinement by molecular docking are shown.

Ser106, Val107, Asn108, Ser118, Asn119, Thr313, His345, Ser349, Leu355, Leu380, Ala404, and Gly410 were involved in hydrophobic interactions.

The residues Arg102, Ser106, Val107, Asn108, Cys407, Thr313, His345, Ser401, Ser349, Val350, and Val351 were found to be common residues interacting with ZINC2358298 studied by all three docking tools. The interactions of OfCYP450–ZINC2358298 complex from Autodock are shown in Figure 2(A).

#### 3.5.4. ZINC8790946

ZINC8790946 formed six hydrogen bonds with Arg102, Val107, Asn250, Val350, Val351, and Cys407 of OfCYP450, with an energy complex of  $-9.03$  Kcal.mol<sup>-1</sup> in Autodock. Additionally, the ZINC8790946 complex was found to be stabilized by hydrophobic interactions with Leu105, Ser106, Asn108, Asn222, Thr313, Ser349, Ser401, Ala404, and Leu446. From Autodock Vina, the complex was stabilized by six



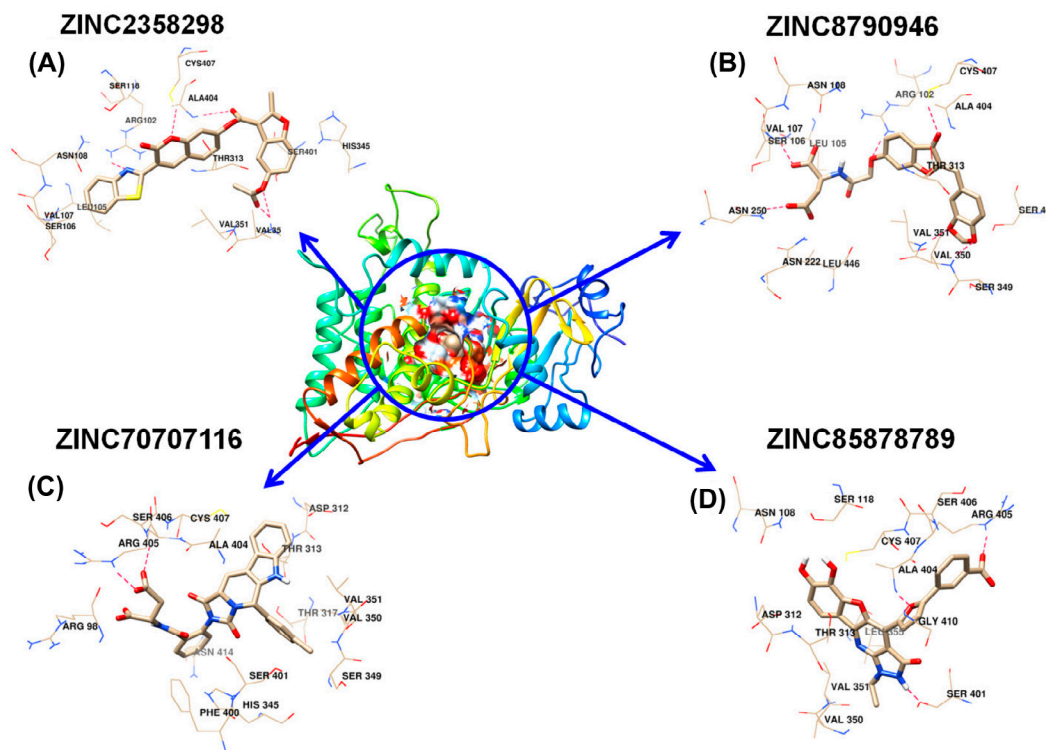


Figure 2. The potential binding pose for the four predicted hits. (A) OfCYP450–ZINC2358298, (B) OfCYP450–ZINC8790946, (C) OfCYP450–ZINC70707116, and (D) OfCYP450–ZINC85878789, binding modes in the active site of OfCYP450 (Four hits are shown in wire form and residues are shown in sticks. The red dotted line represents intermolecular hydrogen bond interactions).

hydrogen bonds with Asn108, Gly403 Ala404, Arg405, Ser406, and Gly410. The residues such as Arg102, Ser118 and Cys407 were found to participate in the hydrophobic interactions. The binding energy of the complex was  $-9.4 \text{ Kcal.mol}^{-1}$  as calculated by Autodock Vina. In MVD analysis, ZINC8790946 formed four hydrogen bonds with Ala404, Arg405, and Gly410, forming an energy complex of  $-194.18$  in MolDock score. Here, residues such as Arg102, Asn108, Ser118, Asn119, Asp312, Thr313, Phe400, Gly403, Ser406, and Cys407 were involved in hydrophobic interactions.

All three docking software suggested that Lys125 Arg102, Asn108, Ala404, and Cys407 were the common residues involved in the interaction between OfCYP450 and ZINC8790946. The interactions of the OfCYP450–ZINC8790946 complex with Autodock are shown in Figure 2(B).

### 3.5.5. ZINC70707116

ZINC70707116 formed a low-energy complex with OfCYP450. It formed two hydrogen bonds with Arg405 and Ser406 of OfCYP450 with an energy complex of  $-10.02 \text{ Kcal.mol}^{-1}$  by Autodock. Additionally, ZINC70707116 was stabilized by hydrophobic interactions with Arg98, Asp312, Thr313, Thr317, His345,

Ser349, Val350, Val351, Phe400, Ser401, Ala404, Cys407, and Asn414. With Autodock Vina, this complex was stabilized by a single hydrogen bond with Gly410 and hydrophobic interactions with Ser301, Asp312, Thr313, Ile344, His345, Val350, Val351, Leu380, Phe400, Gly403, Ala404, Cys407, and Asn414, forming an energy complex of  $-8.3 \text{ Kcal.mol}^{-1}$ . MVD analysis showed that ZINC70707116 formed five hydrogen bonds with Ala404, Arg405, and Cys407, with an energy complex of  $-200.96$  MolDock score. Here, residues such as Arg98, Thr313, Thr317, His345, Val350, His357, Phe400, Ser401, Leu402, Gly403, Ser406, and Gly410 were involved in hydrophobic interactions.

In this docking, Thr313, His345, Phe400, Ala404, and Cys407 were the common residues involved in the interaction between ZINC70707116 with OfCYP450 by all three docking tools. The interactions of OfCYP450–ZINC70707116 complex with Autodock are shown in Figure 2(C).

### 3.5.6. ZINC85878789

ZINC85878789 showed a binding affinity of  $-9.57 \text{ Kcal.mol}^{-1}$  toward OfCYP450 as per Autodock. The complex was stabilized by forming three hydrogen bonds with Ser401, Ala404, and Arg405, while Asn108,

Ser118, Asp312, Ser406, Cys407, Thr313, Val350, Val351, Leu355, and Gly410 were involved in hydrophobic interactions. Autodock Vina showed a binding affinity of  $-10.9 \text{ Kcal.mol}^{-1}$ , and the complex was stabilized by forming four hydrogen bonds with Asn108, Gly403, Ala404, and Cys407 and hydrophobic interactions with Arg102, Asp312, Thr313, Thr317, Ile344, His345, Val351, His357, Phe400, Leu402, Arg405, and Asn414. MVD showed a MolDock score of  $-179.82$  with one hydrogen bond formation with Ala404. Here, Arg102, Asn108, Ser118, Asp312, Thr313, Thr317, Ile344, His345, Val351, His357, Phe400, Leu402, Gly403, Arg405, Cys407, and Asn414 were involved in hydrophobic interactions.

All three docking softwares suggested that Asn108, Asp312, Thr313, Val351, Ala404, Arg405, and Cys407 were the common residues involved in the interaction between OfCYP450 and ZINC85878789. The interactions of the OfCYP450–ZINC85878789 complex in Autodock is shown in Figure 2(D).

### 3.6. Molecular dynamics simulation

MDS is a widely used computational technique for the study of dynamics of any system. It describes the internal motions, conformational changes, and protein–ligand complex stability analysis. In this study, we used MDS for predicting the stability of the predicted hits. Seven systems (one apo-OfCYP450, OfCYP450–itraconazole, OfCYP450–fluconazole, OfCYP450–ZINC2358298, OfCYP450–ZINC8790946, OfCYP450–ZINC70707116, OfCYP450–ZINC85878789) were created and employed for 50 ns time scale MDS study using explicit solvent. All the systems got the equilibration state after 10 ns. Thus, the study was performed using the last 40-ns trajectories.

#### 3.6.1. RMSD

RMSD was used for measuring the scalar distance between atoms. The backbone RMSD of all the systems was calculated. All systems showed stable RMSD value. The RMSD value indicated that after 10 ns, all the systems attained the equilibration state (Figure 3(A)). The average value of RMSD for apo-OfCYP450, OfCYP450–itraconazole, OfCYP450–fluconazole, OfCYP450–ZINC2358298, OfCYP450–ZINC8790946, OfCYP450–ZINC70707116, and OfCYP450–ZINC85878789 were 0.60, 0.25, 0.23, 0.35, 0.26, 0.30, and 0.27 nm, respectively. The reference ligands showed least RMSD value as compared to predicted hits. The complex OfCYP450–ZINC85878789 showed the least RMSD value while OfCYP450–ZINC2358298 showed the highest RMSD value, but all RMSD values were lower than apo-OfCYP450. The RMSD results suggested

that all the systems got the equilibration state and produced stable trajectory for further analysis. RMSF, Rg, hydrogen bonds, principal component analysis, and binding free energy were calculated for the last 40-ns trajectory.

#### 3.6.2. RMSF

RMSF was calculated for each residue of apo-protein and ligand-bound complexes. The higher value of RMSF represented that the structure has some highly flexible regions like loop and turns, while the lower value of RMSF indicated that the structure was good in terms of secondary structure like helix and sheets. We have calculated RMSF value from the last 40-ns equilibrated trajectories and plotted in Figure 3(B). All the complexes showed similar RMSF peak. OfCYP450–ZINC2358298 showed higher RMSF value between 143 and 151 residues. The average RMSF value for apo-OfCYP450, OfCYP450–itraconazole, OfCYP450–fluconazole, OfCYP450–ZINC2358298, OfCYP450–ZINC8790946, OfCYP450–ZINC70707116, and OfCYP450–ZINC85878789 were 0.14, 0.14, 0.13, 0.17, 0.13, 0.15, and 0.11 nm, respectively. The complex OfCYP450–ZINC85878789 showed the least value as compared to other ligands. The RMSF results suggested that ZINC8790946 and ZINC85878789 showed less fluctuation after binding to OfCYP450. The OfCYP450–ZINC2358298 complex showed higher value as compared to other ligand complexes. The OfCYP450–ZINC8790946, OfCYP450–ZINC70707116, and OfCYP450–ZINC85878789 were the best compounds with this result.

#### 3.6.3. Radius of gyration (Rg)

The conformational variations and compactness of the apo-protein and protein–ligand complexes were calculated using Rg. The last 40-ns trajectory were used for the calculation of Rg and shown in Figure 4(A). The average Rg values for apo-OfCYP450, OfCYP450–itraconazole, OfCYP450–fluconazole, OfCYP450–ZINC2358298, OfCYP450–ZINC8790946, OfCYP450–ZINC70707116, and OfCYP450–ZINC85878789 were 2.34, 2.30, 2.32, 2.38, 2.31, 2.31, and 2.33 nm, respectively. OfCYP450–itraconazole showed least Rg value suggesting that this complex is most stable. Our predicted hits also showed similar Rg values. The OfCYP450–ZINC2358298 showed higher Rg value after 18 ns. The Rg peak for OfCYP450–ZINC2358298 increased initially and after that, it showed similar pattern till the end of simulation. The average value of Rg is also high for OfCYP450–ZINC2358298 complex. The OfCYP450–ZINC8790946, OfCYP450–ZINC70707116, and OfCYP450–ZINC85878789 showed lesser values as

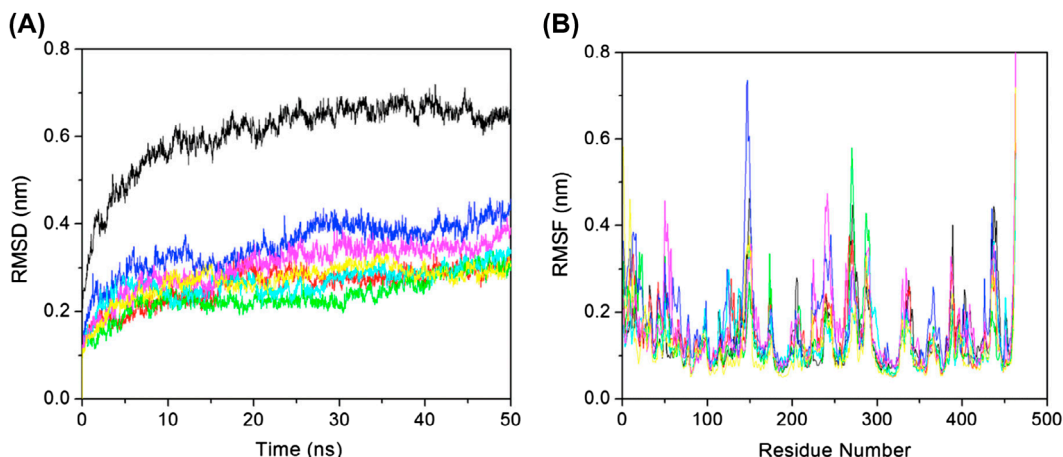


Figure 3. Molecular dynamics simulations. (A) RMSD of the  $C\alpha$  backbone of OfCYP450 (black) and the ligands Itraconazole (red), Fluconazole (yellow), ZINC2358298 (blue), ZINC8790946 (cyan), ZINC70707116 (pink), and ZINC85878789 (yellow) over the 50-ns MDS at 300 K. (B) RMSF of residues during MDS between OfCYP450 (black) and the ligands Itraconazole (red), Fluconazole (yellow), ZINC2358298 (blue), ZINC8790946 (cyan), ZINC70707116 (pink), and ZINC85878789 (yellow).

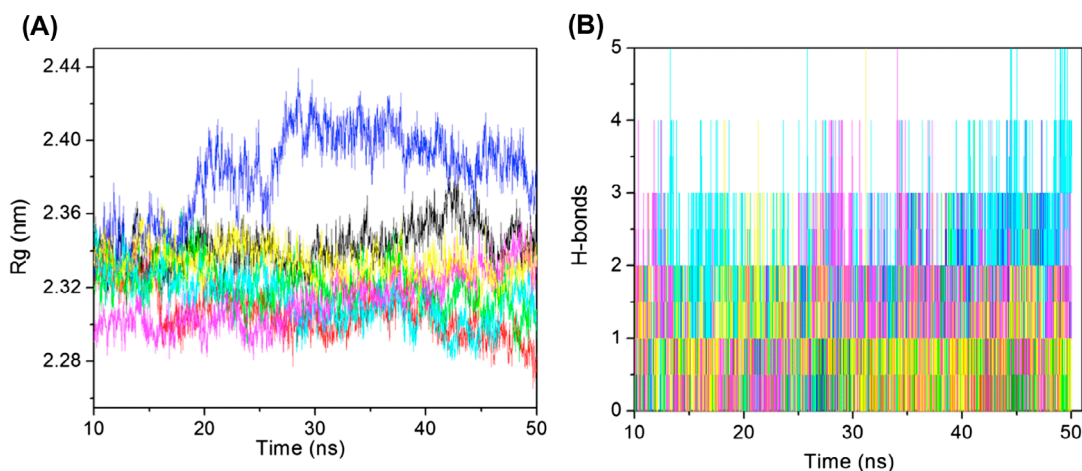


Figure 4. Structural stability analysis. (A) Plot of Radius of gyration vs time for OfCYP450 (black) and the ligand complexes – Itraconazole (red), Fluconazole (yellow), ZINC2358298 (blue), ZINC8790946 (cyan), ZINC70707116 (pink), and ZINC85878789 (yellow). (B) Number of hydrogen bond interactions formed between OfCYP450 and Itraconazole (red), Fluconazole (yellow), ZINC2358298 (blue), ZINC8790946 (cyan), ZINC70707116 (pink), and ZINC85878789 (yellow) complexes during the simulation time.

compared to apo-OfCYP450. The results suggested that the three complexes, OfCYP450–ZINC8790946, OfCYP450–ZINC70707116, and OfCYP450–ZINC85878789, showed more compactness.

#### 3.6.4. Hydrogen bonds

The stability of the protein–ligand complex is maintained by various interactions like hydrogen bonds, hydrophobic interaction, and electrostatic interactions. The hydrogen bonds are the most important bonds for maintaining

the stability of a complex. In this study, we calculated the total number of hydrogen bonds for the last 40-ns trajectory. Figure 4(B) shows the number of hydrogen bonds versus time. Average number of hydrogen bonds for OfCYP450–itraconazole, OfCYP450–fluconazole, OfCYP450–ZINC2358298, OfCYP450–ZINC8790946, OfCYP450–ZINC70707116, and OfCYP450–ZINC85878789 were approximate one for each complex. From the Figure 4(B), it can be seen that OfCYP450–ZINC8790946 and OfCYP450–ZINC70707116 showed more number of hydrogen bonds as compared to the

other complexes, while the reference compounds showed lesser number of hydrogen bonds.

The percent of hydrogen bond occupancy was also calculated for all the predicted hits for the last 40-ns MD trajectories. Ser106 (2.55%), Asn218 (0.30%) were the key residues taking part in hydrogen bond interaction in OfCYP450–itraconazole. Thr317 (0.65%), Ala404 (0.55%), Val351 (0.45%), and Gly410 (0.25%) were the key residues taking part in hydrogen bond interaction in OfCYP450–fluconazole. Arg102 (10.69%), His357 (8.25%), Arg405 (5.35%), and Asp312 (1.15%) were the key residues taking part in hydrogen bond interaction in OfCYP450–ZINC8790946. Cys407 (17.99%), Thr313 (16.54%), Asn119 (4.95%), and Thr317 (1.30%) were the key residues taking part in hydrogen bond interaction in OfCYP450–ZINC2358298, while Ser401 (9.65%), Asn414 (2.05%), Ala404 (1.45%), and Cys407 (1.35%) were the key residues taking part in hydrogen bond interaction in OfCYP450–ZINC70707116. Thr317 (19.69%) and Cys407 (3.90%) formed hydrogen bond interaction with OfCYP450–ZINC85878789. The hydrogen bond occupancy also showed that our predicted hits form more number of hydrogen bonds as compared to the reference compounds.

### 3.6.5. Principal component analysis

The significant motions after ligand binding were calculated using PCA method. It is an established fact that the first few eigenvectors played an important role in the overall motions of protein. For this study, the eigenvectors were calculated by diagonalization of the matrix. The last 40-ns trajectories were used for calculation of eigenvectors. The first 50 eigenvectors were selected for result analysis. Covariance matrix of atomic fluctuations was diagonalized for predicting the eigenvalues. Figure 5(A) represents the eigenvalue in decreasing order versus corresponding eigenvector for apo-OfCYP450, OfCYP450–itraconazole, OfCYP450–fluconazole, OfCYP450–ZINC2358298, OfCYP450–ZINC8790946, OfCYP450–ZINC70707116, and OfCYP450–ZINC85878789. From the 50 eigenvectors, it was observed that the first ten eigenvectors accounted for 80.23, 78.79, 79.31, 84.12, 77.33, 82.77, and 73.22% for apo-OfCYP450, OfCYP450–itraconazole, OfCYP450–fluconazole, OfCYP450–ZINC2358298, OfCYP450–ZINC8790946, OfCYP450–ZINC70707116, and OfCYP450–ZINC85878789, respectively. The reference compounds also showed less motions after binding. It was found that OfCYP450–ZINC70707116 showed higher motions as compared to other complexes. From the PCA, we concluded that OfCYP450–ZINC85878789 and OfCYP450–ZINC8790946 were so far the best-studied complexes.

Another way to achieve the dynamics of system is 2D PCA. In this study, we selected only first two principal components (PCs) for predicting the clear picture of the motions. Figure 5(B) showed the projection of two eigenvectors for reference compounds as well as predicted hits. It was observed that the complex that showed stable cluster and occupied less phase space represented a stable complex while the complex that showed non-stable cluster and occupied more space represented a less stable complex. From the plot, it was found that OfCYP450–ZINC2358298 complex occupied more space and showed less stable cluster as compared to other complexes. The complex OfCYP450–ZINC85878789 showed very stable cluster as compared to the other complexes. The reference compounds also showed stable cluster. The 2D PCA resulted in an agreement with the above result that OfCYP450–ZINC85878789 and OfCYP450–ZINC8790946 were the best studied complexes.

### 3.6.6. Binding free energy analysis

The MM-PBSA tool was used for calculating the binding free energy of protein–ligand complexes. The binding free energies are shown in Table 3. The last 10 ns of MD trajectories were considered for calculating the binding free energy. The OfCYP450–itraconazole, OfCYP450–fluconazole, OfCYP450–ZINC2358298, OfCYP450–ZINC8790946, OfCYP450–ZINC70707116, and OfCYP450–ZINC85878789 showed  $-259.41$  KJ.mol<sup>-1</sup>,  $-110.09$  KJ.mol<sup>-1</sup>,  $-188.25$  KJ.mol<sup>-1</sup>,  $163.30$  KJ.mol<sup>-1</sup>,  $-202.10$  KJ.mol<sup>-1</sup>, and  $-158.79$  KJ.mol<sup>-1</sup> binding free energy, respectively. Furthermore, it was found that the electrostatic interactions, non-polar solvation energy, and van der Waals interactions negatively complimented the overall interaction energy, while the polar solvation energy had positively enriched the binding energy. The reference drug itraconazole showed the highest binding affinity as compared to the predicted hits, while the OfCYP450–ZINC70707116 showed the highest binding followed by OfCYP450–fluconazole, OfCYP450–ZINC2358298, OfCYP450–ZINC8790946, and OfCYP450–ZINC85878789. From the MM-PBSA result, we found that all compounds showed good binding affinity and that OfCYP450–ZINC70707116 was excellent in terms of binding energy.

To quantify the individual amino acid interactions toward total binding free energy, per residue interaction energies were computed using the MM-PBSA approach (Figure 6) for the last 10 ns of MD trajectory. For clear representation of the result, only those residues were selected which actively participated in the binding. The per residue interaction profile revealed that Arg102, Ser106, Val107, Asn108, Lys125, Thr313, His345, Ser349, Val350, Val351, Ser401, and Ala404 were



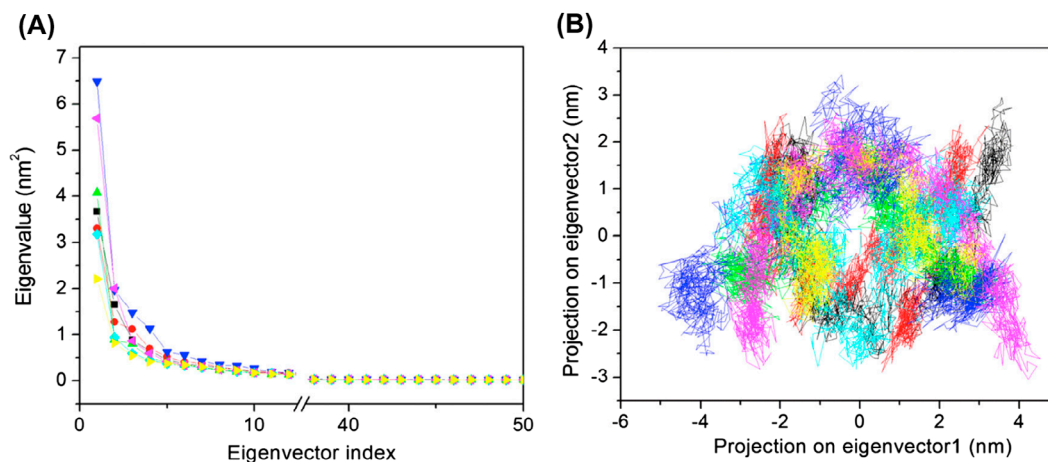


Figure 5. Principal component analysis. (A) Plot of eigenvalues was plotted vs eigenvector index. First 50 eigenvectors were considered. OfCYP450 (black) and the ligands – Itraconazole (red), Fluconazole (yellow), ZINC2358298 (blue), ZINC8790946 (cyan), ZINC70707116 (pink), and ZINC85878789 (yellow) indicate the eigenvalues. (B) Projection of the motion of the protein in phase space along the PC1 and PC2 for OfCYP450 (black) and the ligands Itraconazole (red), Fluconazole (yellow), ZINC2358298 (blue), ZINC8790946 (cyan), ZINC70707116 (pink), and ZINC85878789 (yellow) at 300 K.

Table 3. Table showing the van der Waal, electrostatic, polar salvation, SASA, and binding energy in kJ mol<sup>-1</sup> for four predicted hits.

S. No.	Compound	Van der Waals energy	Electrostatic energy	Polar salvation energy	SASA energy	Binding energy
1.	Itraconazole	-351.04 ± 17.31	33.27 ± 12.71	157.27 ± 23.89	-32.22 ± 1.29	-259.41 ± 17.98
2.	Fluconazole	-155.74 ± 8.24	-18.21 ± 7.12	79.84 ± 9.60	-15.98 ± 0.79	-110.09 ± 10.70
3.	ZINC2358298	-263.41 ± 13.12	-30.77 ± 8.07	130.12 ± 19.99	-24.20 ± 1.21	-188.25 ± 17.10
4.	ZINC8790946	-266.91 ± 12.08	-59.09 ± 9.16	185.83 ± 15.26	-23.13 ± 0.92	-163.30 ± 15.54
5.	ZINC70707116	-284.76 ± 13.75	-18.83 ± 7.53	127.36 ± 16.68	-25.87 ± 1.08	-202.10 ± 16.42
6.	ZINC85878789	-222.54 ± 12.31	-26.19 ± 9.44	112.34 ± 14.73	-22.39 ± 1.09	-158.79 ± 12.84

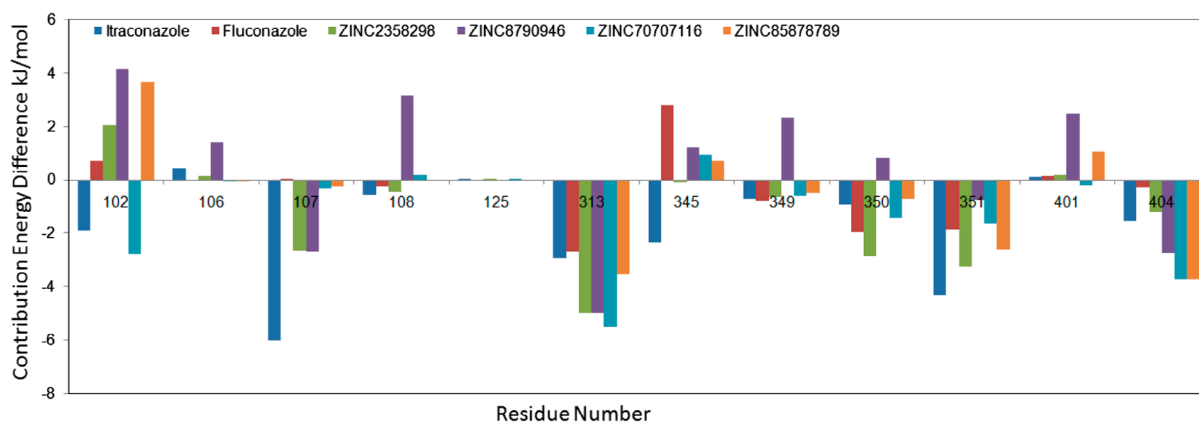


Figure 6. The contributions of individual amino acid residues of OfCYP450 to the total binding energies. Results are shown as the energy contribution differences between the indicated OfCYP450–ligand complexes.

Notes: Negative values indicate a stabilization effect for OfCYP450–ligand interactions, whereas positive values indicate a destabilization effect for OfCYP450–ligand interactions.

actively participating amino acid residues in the predicted hits. From the plot, it can be seen that most residues showed a negative binding affinity, while few

residues showed a positive binding affinity. The residues Arg102, Val107, Thr313, Val350, Val351, and Ala404 showed a negative binding affinity and played an



important role in stabilizing the protein–ligand complex. From the overall result, we found that the predicted hits showed excellent binding energy, and these predicted residues are important for the stability of the protein–ligand complex.

From the overall RMSD, RMSF, Rg, hydrogen bonds, PCA, and binding free energy results, we concluded that OfCYP450–ZINC8790946, OfCYP450–ZINC70707116, and OfCYP450–ZINC85878789 are the best stable complexes that showed excellent binding affinities.

#### 4. Conclusion

In the present work, we screened 1,65,869 compounds against OfCYP450 structure in many rounds. Finally, 361 compounds were selected for ADMET, and from this, we found 10 compounds that were novel in ADMET descriptors. All the selected 10 compounds were docked by multiple docking software, and then four predicted hits were employed for MDS study. Our predicted compounds are equal to itraconazole and better as compare to fluconazole. From MDS, we proposed that ZINC8790946, ZINC70707116, and ZINC85878789 can act as a lead compound against OfCYP450.

#### Supplementary material

The supplementary material for this paper is available online at <https://doi.org/10.1080/07391102.2017.1392897>.

#### Disclosure statement

No potential conflict of interest was reported by the authors.

#### Funding

The study was supported by research grant from the Department of Science and Technology (Grant no. INT/RUS/RFBR/P-200) Govt. of India, India to TT and by the Russian Foundation for Basic Research (Grant no. 15-54-45132 Ind a) to VAM. RS and HS thank the UGC, while PBC thank DST-INSPIRE for providing fellowship. MYP thank to the State Project of Institute of Cytology and Genetics, Siberian Branch of the Russian Academy of Sciences (Project No. 0324-2016-0002). Authors thank the Sulekor supercomputing facility of NEHU, Shillong.

#### References

- Amadei, A., Linssen, A., & Berendsen, H. J. C. (1993). Essential dynamics of proteins. *Proteins*, 17, 412–425.
- Baker, N. A., Sept, D., Joseph, S., Holst, M. J., & McCammon, J. A. (2001). Electrostatics of nanosystems: Application to microtubules and the ribosome. *Proceedings of the National Academy of Sciences*, 98(18), 10037–10041.
- Bowie, J. U., Luthy, R., & Eisenberg, D. (1991). A method to identify protein sequences that fold into a known three-dimensional structure. *Science*, 253(5016), 164–170.
- Cheng, F., Li, W., Zhou, Y., Shen, J., Wu, Z., Liu, G., ... Tang, Y. (2012). admetSAR: A comprehensive source and free tool for assessment of chemical ADMET properties. *Journal of Chemical Information and Modeling*, 52(11), 3099–3105.
- Darden, T., York, D., & Pedersen, L. (1993). Particle mesh Ewald: An N- log (N) method for Ewald sums in large systems. *The Journal of Chemical Physics*, 98(12), 10089–10092.
- Degtyarenko, K. N., & Archakov, A. I. (1993). Molecular evolution of P450 superfamily and P450-containing monooxygenase systems. *FEBS Letters*, 332(1–2)(0014-5793 (Print)), 1–8.
- Denisov, I. G., Makris, T. M., Sligar, S. G., & Schlichting, I. (2005). Structure and chemistry of cytochrome P450. *Chemical Reviews*, 105(6), 2253–2278.
- Devine, C., Brennan, G. P., Lanusse, C. E., Alvarez, L. I., Trudgett, A., Hoey, E., & Fairweather, I. (2010). Inhibition of cytochrome P450-mediated metabolism enhances *ex vivo* susceptibility of *Fasciola hepatica* to triclabendazole. *Parasitology*, 137(5), 871–880.
- DeVore, N. M., Meneely, K. M., Bart, A. G., Stephens, E. S., Battaile, K. P., & Scott, E. E. (2012). Structural comparison of cytochromes P450 2A6, 2A13, and 2E1 with pilocarpine. *FEBS Journal*, 279(9), 1621–1631. doi:10.1111/j.1742-4658.2011.08412.x
- Goodsell, D. S., Morris, G. M., & Olson, A. J. (1996). Automated docking of flexible ligands: Applications of autodock. *Journal of Molecular Recognition*, 9(1), 1–5.
- Gouveia, M. J., Brindley Pj Fau - Santos, L. L., Santos Lj Fau - Correia da Costa, J. M., Brindley Pj Fau - Santos, L. L., Correia da Costa Jm Fau - Gomes, P., Gomes P Fau - Vale, N., & Vale, N. (2013). Mass spectrometry techniques in the survey of steroid metabolites as potential disease biomarkers: A review. *Metabolism*, 1532–8600 (Electronic).
- Hess, B., Bekker, H., Berendsen, H. J., & Fraaije, J. G. (1997). LINCS: A linear constraint solver for molecular simulations. *Journal of Computational Chemistry*, 18(12), 1463–1472.
- Hess, B., Kutzner, C., van der Spoel, D., & Lindahl, E. (2008). GROMACS 4: Algorithms for highly efficient, load-balanced, and scalable molecular simulation. *Journal of Chemical Theory and Computation*, 4(3), 435–447.
- Humphrey, W., Dalke, A., & Schulten, K. (1996). VMD: Visual molecular dynamics. *Journal of Molecular Graphics*, 14(1), 33–38–27–38.
- Klingenberg, M. (1958). Pigments of rat liver microsomes. *Archives of Biochemistry and Biophysics*, 75(2), 376–386.
- Kumari, R., Kumar, R., & Lynn, A. (2014). g\_mmpbsa – a GROMACS tool for high-throughput MM-PBSA calculations. *Journal of Chemical Information and Modeling*, 54(7), 1951–1962.
- Laskowski, R. A., Hutchinson, E. G., Michie, A. D., Wallace, A. C., Jones, M. L., & Thornton, J. M. (1997). PDBsum: A web-based database of summaries and analyses of all PDB structures. *Trends in Biochemical Sciences*, 22(12), 488–490.
- Lim, J. H., Mairiang, E., & Ahn, G. H. (2008). Biliary parasitic diseases including clonorchiasis, opisthorchiasis and fascioliasis. *Abdominal Imaging*, 33(2), 157–165.
- Lun, Z. R., Gasser, R. B., Lai, D. H., Li, A. X., Zhu, X. Q., Yu, X. B., & Fang, Y. Y. (2005). Clonorchiasis: A key foodborne zoonosis in China. *The Lancet Infectious Diseases*, 5(1), 31–41.
- Luthy, R., Bowie, J. U., & Eisenberg, D. (1992). Assessment of protein models with three-dimensional profiles. *Nature*, 356(6364), 83–85. doi:10.1038/356083a0

- Marcos, L. A., Terashima, A., & Gotuzzo, E. (2008). Update on hepatobiliary flukes: Fascioliasis, opisthorchiasis and clonorchiasis. *Current Opinion in Infectious Diseases*, 21(5), 523–530.
- Mas-Coma, S., Bargues, M. D., & Valero, M. A. (2005). Fascioliasis and other plant-borne trematode zoonoses. *International Journal for Parasitology*, 35(11–12), 1255–1278. doi:10.1016/j.ijpara.2005.07.010
- Maule, A. G., & Marks, N. J. (2006). *Parasitic flatworms: Molecular biology, biochemistry, immunology and physiology*: CABI.
- Mordvinov, V. A., & Furman, D. P. (2010). The digenea parasite *Opisthorchis felineus*: A target for the discovery and development of novel drugs. *Infectious Disorders – Drug Targets*, 10(5), 385–401.
- Mordvinov, V. A., Shilov, A. G., & Pakharukova, M. Y. (2017). Anthelmintic activity of cytochrome P450 inhibitors miconazole and clotrimazole: *In-vitro* effect on the liver fluke *Opisthorchis felineus*. *International Journal of Antimicrobial Agents*, 50(1), 97–100.
- Nebert, D. W., & Russell, D. W. (2002). Clinical importance of the cytochromes P450. *The Lancet*, 360(9340), 1155–1162.
- Oostenbrink, C., Villa, A., Mark, A. E., & Van Gunsteren, W. F. (2004). A biomolecular force field based on the free enthalpy of hydration and solvation: The GROMOS force-field parameter sets 53A5 and 53A6. *Journal of Computational Chemistry*, 25(13), 1656–1676.
- Pakharukova, M. Y., Ershov, N. I., Vorontsova, E. V., Katokhin, A. V., Merkulova, T. I., & Mordvinov, V. A. (2012). Cytochrome P450 in fluke *Opisthorchis felineus*: Identification and characterization. *Molecular and Biochemical Parasitology*, 181(1872–9428 (Electronic)), 190–194.
- Pakharukova, M. Y., & Mordvinov, V. A. (2016). The liver fluke *Opisthorchis felineus*: Biology, epidemiology and carcinogenic potential. *Transactions of The Royal Society of Tropical Medicine and Hygiene*, 110(1), 28–36.
- Pakharukova, M. Y., Shilov, A. G., Pirozhkova, D. S., Katokhin, A. V., & Mordvinov, V. A. (2015). The first comprehensive study of praziquantel effects in vivo and in vitro on European liver fluke *Opisthorchis felineus* (Trematoda). *International Journal of Antimicrobial Agents*, 46(1), 94–100.
- Pakharukova, M. Y., Vavilin, V. A., Sripa, B., Laha, T., Brindley, P. J., & Mordvinov, V. A. (2015). Functional analysis of the unique cytochrome P450 of the liver fluke *Opisthorchis felineus*. *PLoS Neglected Tropical Diseases*, 9, 1935–2735 (Electronic).
- Pandey, T., Shukla, R., Shukla, H., Sonkar, A., Tripathi, T., & Singh, A. K. (2016). A combined biochemical and computational studies of the rho-class glutathione s-transferase sll1545 of *Synechocystis* PCC 6803. *International Journal of Biological Macromolecules*, 94(Pt A), 378–385. doi:10.1016/j.ijbiomac.2016.10.040
- Pathak, R. K., Baunthiyal, M., Shukla, R., Pandey, D., Taj, G., & Kumar, A. (2017). In silico identification of mimicking molecules as defense inducers triggering jasmonic acid mediated immunity against alternaria blight disease in brassica species. *Frontiers in Plant Science*, 8, 609. doi:10.3389/fpls.2017.00609
- Pettersen, E. F., Goddard, T. D., Huang, C. C., Couch, G. S., Greenblatt, D. M., Meng, E. C., & Ferrin, T. E. (2004). UCSF Chimera—a visualization system for exploratory research and analysis. *Journal of Computational Chemistry*, 25(13), 1605–1612. doi:10.1002/jcc.20084
- Pronk, S., Pall, S., Schulz, R., Larsson, P., Bjelkmar, P., Apostolov, R., ... Lindahl, E. (2013). GROMACS 4.5: A high-throughput and highly parallel open source molecular simulation toolkit. *Bioinformatics*, 29(7), 845–854.
- Reynald, R. L., Sansen, S., Stout, C. D., & Johnson, E. F. (2012). Structural characterization of human cytochrome P450 2C19: Active site differences between P450s 2C8, 2C9, and 2C19. *Journal of Biological Chemistry*, 287(53), 44581–44591. doi:10.1074/jbc.M112.424895
- Ryckaert, J., Ciccotti, G., & Berendsen, H. J. C. (1977). Numerical integration of the cartesian equations of motion of a system with constraints: Molecular dynamics of n-alkanes. *Journal of Computational Physics*, 23(3), 327–341.
- Schoch, G. A., Yano, J. K., Sansen, S., Dansette, P. M., Stout, C. D., & Johnson, E. F. (2008). Determinants of cytochrome P450 2C8 substrate binding: Structures of complexes with montelukast, troglitazone, felodipine, and 9-cis-retinoic acid. *Journal of Biological Chemistry*, 283(25), 17227–17237. doi:10.1074/jbc.M802180200
- Schuttelkopf, A. W., & van Aalten, D. M. (2004). PRODRG: A tool for high-throughput crystallography of protein-ligand complexes. *Acta Crystallographica Section D Biological Crystallography*, 60(Pt 8), 1355–1363.
- Shukla, R., Shukla, H., Sonkar, A., Pandey, T., & Tripathi, T. (2017). Structure-based screening and molecular dynamics simulations offer novel natural compounds as potential inhibitors of *Mycobacterium tuberculosis* isocitrate lyase. *Journal of Biomolecular Structure and Dynamics*, 1–106. doi:10.1080/07391102.2017.1341337
- Shukla, H., Shukla, R., Sonkar, A., Pandey, T., & Tripathi, T. (2017). Distant Phe345 mutation compromises the stability and activity of *Mycobacterium tuberculosis* isocitrate lyase by modulating its structural flexibility. *Scientific Reports*, 7(1), 1058. doi:10.1038/s41598-017-01235-z
- Shukla, H., Shukla, R., Sonkar, A., & Tripathi, T. (2017). Alterations in conformational topology and interaction dynamics caused by L418A mutation leads to activity loss of *Mycobacterium tuberculosis* isocitrate lyase. *Biochemical and Biophysical Research Communications*, 490(2), 276–282. doi:10.1016/j.bbrc.2017.06.036
- Sithithaworn, P., Nuchjungreed, C., Srisawangwong, T., Ando, K., Petney, T. N., Chilton, N. B., & Andrews, R. H. (2007). Genetic variation in *Opisthorchis viverrini* (Trematoda: Opisthorchiidae) from northeast Thailand and Laos PDR based on random amplified polymorphic DNA analyses. *Parasitol Res*, 100(3), 613–617.
- Sonkar, A., Shukla, H., Shukla, R., Kalita, J., Pandey, T., & Tripathi, T. (2017). UDP-N-Acetylglucosamine enolpyruvyl transferase (MurA) of *Acinetobacter baumannii* (AbMurA): Structural and functional properties. *International Journal of Biological Macromolecules*, 97, 106–114. doi:10.1016/j.ijbiomac.2016.12.082
- Sripa, B., Kaewkes, S., Sithithaworn, P., Mairiang, E., Laha, T., Smout, M., ... Brindley, P. J. (2007). Liver fluke induces cholangiocarcinoma. *PLoS Medicine*, 4(7), e201.
- Tchuente, L. A., Shaw, D. J., Polla, L., Cioli, D., & Vercruyse, J. (2004). Efficacy of praziquantel against *Schistosoma haematobium* infection in children. *The American Journal of Tropical Medicine and Hygiene*, 71(6), 778–782.
- Thomsen, R., & Christensen, M. H. (2006). MolDock: A new technique for high-accuracy molecular docking. *Journal of Medicinal Chemistry*, 49(11), 3315–3321.
- Trott, O., & Olson, A. J. (2010). AutoDock Vina: Improving the speed and accuracy of docking with a new scoring function, efficient optimization, and multithreading. *Journal of Computational Chemistry*, 31(2), 455–461.

- Vale, N., Gouveia Mj Fau - Botelho, M., Botelho M Fau - Sripa, B., Sripa B Fau - Suttiprapa, S., Suttiprapa S Fau - Rinaldi, G., Rinaldi G Fau - Gomes, P., ... Correia da Costa, J. M. (2013). Carcinogenic liver fluke *Opisthorchis viverrini* oxysterols detected by LC-MS/MS survey of soluble fraction parasite extract. *Parasitology International*, 1873–0329 (Electronic).
- WHO. (2008). *WHO model formulary*. Geneva: Author.
- Wiederstein, M., & Sippl, M. J. (2007). ProSA-web: Interactive web service for the recognition of errors in three-dimensional structures of proteins. *Nucleic Acids Research*, 35 (Web Server), W407–W410. doi:10.1093/nar/gkm290
- Wilderman, P. R., Shah, M. B., Jang, H. H., Stout, C. D., & Halpert, J. R. (2013). Structural and thermodynamic basis of (+)-alpha-pinene binding to human cytochrome P450 2B6. *Journal of the American Chemical Society*, 135(28), 10433–10440. doi:10.1021/ja403042k
- Ziniel, P. D., Karumudi, B., Barnard, A. H., Fisher, E. M., Thatcher, G. R., Podust, L. M., & Williams, D. L. (2015). The *Schistosoma mansoni* Cytochrome P450 (CYP3050A1) is essential for worm survival and egg development. *PLoS Neglected Tropical Diseases*, 9, 1935–2735 (Electronic). doi:10.1021/ja403042k